JBC Papers in Press. Published on January 8, 2013 as Manuscript M112.409789
The latest version is at http://www.jbc.org/cgi/doi/10.1074/jbc.M112.409789

Structural and Functional Similarities of Calcium Homeostasis Modulator 1 (CALHM1) Ion Channel With Connexins, Pannexins and Innexins

Adam P. Siebert[1], Zhongming Ma[1], Jeremy D. Grevet[1], Angelo Demuro[2], Ian Parker[2] and J. Kevin Foskett[1,3,*]

Departments of [1]Physiology, and [3]Cell and Developmental Biology
Perelman School of Medicine
University of Pennsylvania, Philadelphia, PA 19104-6085

[2]Department of Neurobiology and Behavior
University of California, Irvine, CA 92697

Running title: Similarities of CALHM1, connexins, pannexins-innexins

To whom correspondence should be addressed: J. Kevin Foskett, Department of Physiology, 726 Clinical Research Bldg., 415 Curie Blvd., University of Pennsylvania, Philadelphia, PA 19104-6085, Phone: (215) 898-1354, email: foskett@mail.med.upenn.edu

Keywords: Permeation, Gap Junction, Photobleaching, Single molecule, Topology, Dye Transfer

Background: CALHM1 is an ion channel for which structural information is lacking.
Results: CALHM1 has poor ion selectivity, a wide (~ 14 Å) pore and is a hexamer, with monomers having four transmembrane domains with cytoplasmic termini.
Conclusions: CALHM1 shares structural features with pannexins, connexins and innexins.
Significance: CALHMs, connexins, pannexins-innexins are three structurally related protein families with shared and distinct functional properties.

SUMMARY

CALHM1 (calcium homeostasis modulator 1) forms a plasma membrane ion channel that mediates neuronal excitability in response to changes in extracellular Ca^{2+} concentration. Six human CALHM homologs exist with no homology to other proteins, although CALHM1 is conserved across >20 species. Here we demonstrate that CALHM1 shares functional and quaternary and secondary structural similarities with connexins and evolutionarily distinct innexins and their vertebrate pannexin homologs. A CALHM1 channel is a hexamer, comprised of six monomers, each of which possesses four transmembrane domains, cytoplasmic amino- and carboxyl termini, an amino terminal helix, and conserved extracellular cysteines. The estimated pore diameter of CALHM1 channel is ~14 Å, enabling permeation of large charged molecules. Thus, CALHMs, connexins, and pannexins and innexins are protein families structurally related with shared and distinct functional properties.

CALHM1 (calcium homeostasis modulator 1), a gene of unknown function, was identified as a possible modifier of the age of onset of Alzheimer's disease (1,2). CALHM1 encodes a glycosylated membrane protein expressed throughout the brain that lacks significant homology to other proteins. Six human CALHM homologs have been identified, with alternatively spliced variants and different expression patterns throughout the body, and CALHM1 is conserved across > 20 species, including vertebrates as well as urochordates, hemichordates and nematodes. Recently, CALHM1 was shown to form a novel Ca^{2+} permeable ion channel whose gating is allosterically regulated by both membrane voltage and extracellular Ca^{2+} concentration ($[Ca^{2+}]_o$) (3). CALHM1 ion channels were shown to mediate enhanced neuronal excitability in response to

reduced $[Ca^{2+}]_o$ that occurs in the brain in physiological and pathological situations (3). Cortical neurons from mice with *CALHM1* genetically deleted have altered electrophysiological properties and fail to respond to reduced $[Ca^{2+}]_o$ (3). Notably, CALHM1 is permeable to Ca^{2+} (1,3) and may also participate in cytoplasmic Ca^{2+} homeostasis (1,3-5).

The ion permeability properties of CALHM1 are unique: Ca^{2+} is only 10-fold selected for over Na^+ (P_{Ca} : P_{Na} ~11), CALHM1 does not discriminate between Na^+ and K^+, and it allows significant monovalent anion permeation (P_{Cl} : P_{Na} ~ 0.5) (3). To understand the permeation properties of the CALHM1 ion channel in more detail, we examined permeation of different monovalent and divalent cations as well as different sized structurally-similar ions using electrophysiological and optical imaging techniques. Both approaches indicate that the CALHM1 pore has a surprisingly wide diameter, comparable to that of gap-junction forming connexins. Furthermore, we show that, like connexons, a CALHM1 ion channel is a hexamer of CALHM1 monomers, each of which contains four transmembrane domains with cytoplasmic amino- and carboxyl-termini. Together, these functional and structural features suggest that CALHM1 belongs to a third protein family that is similar to connexins and pannexins-innexins.

EXPERIMENTAL PROCEDURES

Cell Culture and Transfection. Neuro-2a (N2a) mouse neuroblastoma cells were cultured in Eagle's Minimum Essential medium supplemented with 10% fetal bovine serum and 0.5x penicillin-streptomycin (Invitrogen) at 37ºC, 5% CO_2. For all imaging experiments, cells were plated on glass coverslips one day prior to transfection. SH-SY5Y cells were maintained in a 1:1 mixture of ATCC-formulated Eagle's Minimum Essential Medium and F12 medium, supplemented with 10% FBS and 0.5x penicillin-streptomycin in 95% air/5% CO_2 at 37ºC. Human wild-type (WT) CALHM1 was subcloned into pIRES2-EGFP (Clontech), pEGFPN1 (Clontech), pcDNA3.1-Myc-His version B (Invitrogen), and pBF (provided by F. Ashcroft, Oxford, UK) vectors. CALHM1-GFP was subcloned from pEGFPN1 into pBF. N2a and SH-SY5Y cells were transfected using Lipofectamine 2000 (Invitrogen).

Electrophysiology. All electrophysiological recordings were performed at room temperature (20-23ºC). cRNA was *in vitro* transcribed from linearized plasmids with the mMessage mMachine kit (Ambion). Female *Xenopus laevis* were purchased from Xenopus One. Oocytes were defolliculated by treatment with collagenase (Worthington Biochemical Corp.). At least 2 hr after collagenase treatment, 1-5 ng of CALHM1 cRNA was injected into oocytes with 80 ng of *Xenopus* connexin38 antisense oligonucleotide to inhibit endogenous Cx38 currents (3,6,7). Oocytes were kept at 16ºC in a ND96 solution (in mM: 96 NaCl, 2 KCl, 1.8 $CaCl_2$, 1 $MgCl_2$, 2.5 Na-pyruvate, 5 HEPES, 1x penicillin-streptomycin, and pH 7.6 (adjusted by NaOH)). Recordings were performed 3-5 days after injection. Oocytes used in two-electrode voltage (TEV) clamp experiments were injected with a 50 nL mixture of 20 mM BAPTA and 10 mM Ca^{2+} at least 30 min prior to recording to clamp $[Ca^{2+}]_i$ to ~100 nM and minimize activation of endogenous Ca^{2+}-activated Cl^- currents (3). In divalent cation-free solutions, 0.5 mM EGTA and 0.5 mM EDTA were added to the bath solutions without adding divalent cations. In ion permeability experiments, sucrose was used as a substitute for NaCl or Ca^{2+} to maintain osmolarity.

Data were acquired with an OC-725C amplifier (Warner Instrument Corp.) at 1 kHz with 16-bit A/D converter (Instrutech ITC-16). Electrodes were made from thin-walled TW100F-6 glass (World Precision Instruments, Inc.), filled with 3 M KCl, and connected by 3 M KCl agar bridges to the bath solution.

Two different voltage protocols were used during this study. In the absence of divalent cations, CALHM1 channels have fast activation gating and cannot be closed even at very negative voltages (3). A Divalent-Free Voltage protocol (DFV protocol) (Fig. 1A) was designed to determine the instantaneous current-voltage relations. Oocytes were clamped at resting membrane potential (RMP) that was measured at the beginning of each experiment. A short (250 ms) depolarization to +60 mV from RMP activated CALHM1 channels. The voltage was then immediately stepped to test pulses ranging

from -80 to +40 mV in 10 mV increments every 15 sec to record the instantaneous currents. When oocytes are bathed in divalent cation-containing solutions, activation gating is slowed and CALHM1 is stabilized in closed states (3). A Divalent Voltage protocol (DV protocol) (Fig. 1B) was used to determine the instantaneous I-V relations. Oocytes were clamped at a holding potential of -40 mV to close CALHM1 channels. A 2000 ms depolarization to +60 mV from –40 mV activated CALHM1. The voltage was then immediately stepped to test potentials from -80 to + 40 mV in 10 mV increments every 15 sec to measure the instantaneous currents. One additional step to -80 mV for 1000 ms was applied to ensure lack of non-specific leak during this protocol.

Relative Permeability Estimation. Relative permeabilities of K^+ and Cl^- (P_K/P_{Na} and P_{Cl}/P_{Na} , respectively) were estimated from reversal potentials (E_{rev}) using the Goldman-Hodgkin-Katz (GHK) constant field equation:

$$E_{rev} = \frac{RT}{F}\ln\frac{P_K[K^+]_o + P_{Na}[Na^+]_o + P_{Cl}[Cl^-]_i}{P_K[K^+]_i + P_{Na}[Na^+]_i + P_{Cl}[Cl^-]_o}, \textbf{(Eqn 1)}$$

where subscripts *i* and *o* denote intracellular and extracellular, respectively; *R*, *T*, and *F* have their usual meanings, and P_{Na}, P_K, and P_{Cl} are the membrane permeabilities to Na^+, K^+, and Cl^-, respectively. For estimations of the relative divalent cation (M^{2+}) permeability, the GHK equation can be derived to an extended constant-field equation:

$$E_{rev} = \frac{RT}{F}\ln\frac{-b+\sqrt{b^2-4ac}}{2a}$$

where

$$a = [Na^+]_i + \frac{P_{Cl}}{P_{Na}}[Cl^-]_o + 4\frac{P_M}{P_{Na}}[M^{2+}]_i + \frac{P_K}{P_{Na}}[K^+]_i + \frac{P_{MES}}{P_{Na}}[MES^-]_o + \frac{P_X}{P_{Na}}[X^+]_i$$

$$b = ([Na^+]_i - [Na^+]_o) - \frac{P_{Cl}}{P_{Na}}([Cl^-]_i - [Cl^-]_o) + \frac{P_K}{P_{Na}}([K^+]_i - [K^+]_o) - \frac{P_{MES}}{P_{Na}}([MES^-]_i - [MES^-]_o) + \frac{P_X}{P_{Na}}([X^+]_i - [X^+]_o)$$

$$c = -[Na^+]_o - \frac{P_{Cl}}{P_{Na}}[Cl^-]_i - \frac{P_K}{P_{Na}}[K^+]_o - 4\frac{P_M}{P_{Na}}[M^{2+}]_o - \frac{P_{MES}}{P_{Na}}[MES^-]_i - \frac{P_X}{P_{Na}}[X^+]_o$$

(*Eqn 2*)

where X^+ is any other monovalent cation except Na^+ and K^+, and P_{Na}, P_K, P_{Cl}, P_{MES}, P_X, and P_M are the membrane permeabilities to Na^+, K^+, Cl^-, MES^-, X^+, and M^{2+}, respectively. The cytoplasmic ionic concentrations of Na^+, K^+, Cl^-, and Ca^{2+} were assumed to be (in mM) 7, 98, 37, and 3×10^{-4}, respectively (8). Both equations assume that the membrane is a homogeneous slab of material into which permeant particles partition instantaneously from the bulk solution, the ions cross the membrane independently, the electric field is constant (9), and the intracellular ionic concentrations do not change during the protocols.

Ionic Activity. When oocytes were bathed in solutions containing divalent cations, the ionic activities of the divalent cations were used instead of concentration. The ionic activity was calculated using (10):

$$a_{ion} = \gamma_z c_{ion}, \textbf{(Eqn 3)}$$

where

$$\log\gamma_z = \frac{-|z_+ z_-|A\sqrt{I}}{1+Bs\sqrt{I}}, \textbf{(Eqn 4)}$$

where γ is the activity coefficient, z is the valence of the ion, A and B are constants that equal 0.5108 and 0.3287 at 25ºC respectively, and I is the ionic strength.

$$I = \frac{1}{2}\sum_i z_i^2 c, \textbf{(Eqn 5)}$$

where z is the ionic valence and c is the molar concentration.

Pore Size. Two estimates of pore diameter were made using the excluded volume model (11-14). Assuming a circular pore and spherical amines, the relationship between the relative permeability and ionic radius is:

$$\frac{P_X}{P_{Na}} = A\left(1 - \frac{a}{r}\right)^2, \textbf{(Eqn 6)}$$

where P_X/P_{Na} is the relative permeability, a is the radius of the amine compound, r is the radius of the pore, and A is a scaling factor. The second model includes a term for the viscous drag of the amine as a function of the size of the amine (a). This model is defined as:

$$\frac{P_X}{P_{Na}} = \frac{\left(A\left(1 - \frac{a}{r}\right)^2\right)}{a}, \textbf{(Eqn 7)}$$

where all terms are the same as above.

CALHM1 Current Pharmacology. CALHM1-expressing oocytes bathed in 5 mM Ca^{2+} solution were clamped at a holding membrane potential of -15 mV. CALHM1 currents induced by exposure to a nominally Ca^{2+}-free solution containing 1 mM Mg^{2+} were measured in response to test pulses to -80 mV for 25 ms every 5 sec. Following 180 sec of exposure to nominally Ca^{2+}-free solution, test agents were perfused into the bath for 180 sec. 100 μM Gd^{3+} was applied for 180 sec after perfusion of the tested agents, and the currents were normalized to those immediately preceding application of the test agents for each experiment. Averaged normalized currents (mean ± s.e.m.) are shown.

Fluorescent Dye Uptake. N2a cells were transiently transfected with CALHM1 or empty vector. Experiments were performed 16-24 hr post-transfection. Since Ca^{2+}_o modulates the gating of CALHM1, cells were incubated in dye-containing (0.1 mg/ml) Hanks' Balanced Saline Solution (HBSS) for 8 min with Ca^{2+} (5 mM) to keep CALHM1 in closed states and thus inhibit dye uptake. The cells were then washed in 5 mM Ca^{2+} HBSS without dye to wash away excess extracellular dye. Alternatively, to activate CALHM1, cells were washed with HBSS containing 0.5 mM EGTA for 1 min. Then cells were incubated in nominally divalent cation free HBSS containing dye (0.1 mg/ml) for 5 min. The cells were then incubated in dye-containing (0.1 mg/ml) HBSS with Ca^{2+} (5 mM) for 3 min to close CALHM1 and trap the dye inside the cells. Finally, the cells were washed in 5 mM Ca^{2+} HBSS without dye to remove excess extracellular dye. DIC and fluorescence images were taken using the appropriate optical filters to visualize each dye.

Fluorescence images were analyzed using ImageJ. The plasma membranes of healthy cells were traced on the DIC images to establish the regions of interest (ROI) of a particular field of cells. The same ROIs were used in the corresponding fluorescence image to measure the average fluorescent intensity of each cell. The off-cell background fluorescence was subtracted from the fluorescence of each cell to correct for any residual dye that had not been sufficiently washed away. A box plot was generated for each cell category for each dye. Since the fluorescent intensities of the CALHM1-activated cells were not normally distributed, the Kruskal-Wallis Test was used to determine statistical significance of median fluorescent intensities with an adjusted p-value due to the multiple comparisons.

Western Blotting. 16-24 hr after transfection, cells were lysed in standard lysis buffer (250 mM NaCl, 50 mM Tris pH 8.0, 1% Triton X-100, and a protease and phosphatase inhibitor mixture (PhosSTOP; Roche)). Samples were bath sonicated at 4ºC for 10 min and then centrifuged at 14,000 x *g* for 10 min. Supernatants were used to determine protein concentrations (Bio-Rad DC protein assay method). 4x Sample Buffer (8% SDS, 40% glycerol, 250 mM Tris pH 6.8, and 0.002% bromphenol blue) was added to each sample before being boiled for 10 min. The percentage of β-mercaptoethanol (βME) was varied between 0.5 % and 8%. Proteins were separated by SDS-PAGE on 10% Tris-HCl gels, transferred to nitrocellulose membranes, and blocked at room temperature for 1 hr in Tris-

buffered saline (50 mM Tris/HCl, 150 mM NaCl; pH 7.6) containing 0.1% Tween-20 (TBST) with 5% nonfat milk. Membranes were washed in TBST and incubated overnight at 4ºC with primary antibody in 5% milk/TBST. The CALHM1 antibody (gift from P. Marambaud; specifically recognizes the sequence 319-EPPLMGNGWA-328) concentration was 1:250, the tubulin antibody (Invitrogen 32-2600) concentration was 1:2000. Membranes were incubated for 1 hr at room temperature with secondary antibody (goat anti-mouse, 1:5,000 dilution in 5% milk/TBST) conjugated to HRP, followed by chemiluminescence detection (ECL-Plus reagent; Pierce) and exposure to HyBlot CL (Denville Scientific). To ensure equal loading, membranes were submerged in stripping buffer (Restore Western blot stripping buffer; Pierce) at 37ºC for 20 min, and then re-probed with a loading control antibody, ß-tubulin. Films were scanned.

Blue Native PAGE. Blue Native PAGE (BN-PAGE) western blotting was performed according to Invitrogen's recommended protocols. NativePage™ reagents were acquired from Invitrogen. Transiently-transfected SH-SY5Y cells were lysed in standard lysis solution (250 mM NaCl, 50 mM TRIS pH 8.0, and 1% Triton X-100). Appropriate volumes of NativePAGE™ sample Buffer (Invitrogen) were added, and appropriate volume of NativePAGE™ G-250 Sample Additive was introduced immediately before loading on a NativePAGE™ Novex® 3-12% Bis-Tris Gel. NativeMark™ Unstained Protein Standard was added to the gel to estimate molecular mass. The Dark Blue Cathode Buffer was used until the dye front migrated through the first third of the gel. It was replaced with the Light Blue Cathode Buffer and electrophoresis continued. The gel was run at 150V for the first 60 min, and then 250V for the remainder of the time. Following electorophoresis, proteins were transferred to PVDF membranes using NuPAGE® Transfer Buffer at 180 mA for 60 min to transfer higher molecular mass proteins at 4ºC. The proteins were fixed on the membrane by shaking the membrane in 8% acetic acid for 15 min. Acetic acid was removed by rinsing the membrane in deionized water. Background dye was removed by shaking in methanol followed by washing in water. Standard western blotting techniques, described above, were used to detect CALHM1.

Single Molecule Photobleaching. Single-molecule bleaching experiments were performed as described (15). Defolliculated *Xenopus* oocytes were injected with cRNAs for human CALHM1-GFP 12-24 hr before imaging. Individual CALHM1-GFP puncta were visualized by TIRF microscopy using a home-built system (16) based on an Olympus IX70 microscope equipped with a ×60, NA 1.45 TIRF objective. Devitellinated oocytes were allowed to settle on a cover glass forming the base of the recording chamber and were bathed in calcium-free Ringer's solution (composition in mM: NaCl, 120; KCl, 2; $MgCl_2$, 5; EGTA, 1, HEPES, 5; pH 7.4). GFP-tagged molecules lying within the ~100 nm evanescent field were excited by total internal reflection of a 488 nm laser beam incident through the microscope objective. Images (128×128 pixel; 1 pixel = 0.33 μm) were acquired at 10 frames s^{-1} by a Cascade 128+ electron multiplying CCD camera (Roper Scientific).

The resulting image stacks were processed in MetaMorph (Molecular Devices) by subtraction of a heavily smoothed (7×7 pixel) copy of each frame to correct for bleaching of autofluorescence and other background signals. Traces such as those in Fig. 3D (black data points) were then obtained from selected spots, excluding those that showed obvious movement or where spots were too close to be unambiguously separated. The number of bleaching steps in each trace was determined using the StepFinder algorithm, devised originally to find steps of single molecular motors (17), that assumes only that the data is a train with steps of varying size and duration, hidden in Gaussian noise. Previous reports have shown that the amplitudes of successive bleaching steps recorded from mulitmeric-tagged proteins vary (18-21). We also detected photobleaching steps by visual inspection (15,18,22,23), with measurements restricted to those spots that showed complete bleaching and where fluorescence steps could be clearly resolved above the noise level. A bleaching step was defined as an abrupt (≤ 2 frames) change in fluorescence between dwell states during which the intensity fluctuated within the noise level around a stable value for ≥ 3 frames (18).

The observed distribution of the number of bleaching steps was fitted with a binomial distribution:

$$\text{percentage of particles} = \frac{\binom{Total}{Steps} Bright^{Steps}(1-Bright)^{(Total-Steps)}}{1-(1-Bright)^{Total}}, \quad \textbf{(Eqn 8)}$$

where *Total* = the total number of monomers in the multimer, *Steps* = the number of photobleaching steps, and *Bright* = the percentage of GFP molecules that is fluorescent.

Immunostaining. PC12 cells were transiently transfected with pIRES-CALHM1-EGFP2 or pIRES-EGFP2 alone. Two methods of immunostaining were used to distinguish between cytoplasmic or extracellular location of an epitope. For the permeabilized cell method, cells were washed twice with PBS at 4ºC, then fixed on ice with 4% paraformaldehyde for 20 min followed by permeabilization for 30 min with 0.2% saponin at room temperature. Cells were washed twice with PBS before incubating in primary antibody for 1 hr at 4ºC, then washed three times in PBS and incubated in secondary antibody (Alexa-Fluor secondary antibody) for 1 hr at room temperature. Finally, cells were washed 3 times in PBS at room temperature. Cells were counterstained with DAPI. Using the unpermeabilized cell immunostaining protocol, cells were washed twice in PBS + 1% BSA, incubated in primary antibody for 1 hr at 4ºC, and washed twice in PBS before being fixed in 4% paraformaldehyde for 20 min at 4ºC. The cells were washed three times in PBS and then incubated in secondary antibody for 1 hr at room temperature, washed three times in PBS at room temperature and counterstained with DAPI. Control experiments, performed on cells expressing GFP (an intracellular epitope) or cells expressing 3xHA-OCA2 (an epitope that is known to be in extracellular regions of OCA2 (24)), validated the methods (data not shown).

Fluorescent Dye Transfer. Transiently-transfected (GFP, pIRES-CALHM1-GFP, or GFP-tagged Cx30) N2a cells, plated on glass coverslips, were visualized on a fixed stage fluorescence microscope and identified by expression of GFP. The cells were bathed in physiological extracellular solution (in mM: 150 Na^+, 5.4 K^+, 20 glucose, 1.5 Ca^{2+}, 1 Mg^{2+}, 150 Cl^-, 10 HEPES, pH 7.4). Alexa350 (2 mM) was dissolved in a patch pipette solution (in mM: 140 K^+, 5 Na^+, 10 Cl^-, 2 $MgCl_2$, 1 EGTA, 10 HEPES, 4 MgATP, 2 phosphocreatine, pH 7.3). The electrode tips were backfilled with dye solution and used to patch a single transfected cell within a cluster of transfected cells. After achieving the whole-cell configuration, dye diffused into the cell for 5 min while holding at -20 mV. The cells were imaged in epifluorescence microscopy 5-60 min after dye loading (340/10 nm excitation filter, 410 nm dichroic, 460/50 nm emission filter) to assess the extent of dye transfer. Dye was transferred if more than one cell in the cluster had Alexa350 fluorescence.

RESULTS

CALHM1 Has Weak Ion Selectivity–To examine the permeability properties of CALHM1 channels, whole-cell instantaneous currents were recorded using either the DFV (Fig. 1A) or DV (Fig. 1B) protocols from oocytes expressing CALHM1. Representative families of current traces elicited in the absence or presence of divalent cations are shown in Fig. 1C and 1D, respectively. The instantaneous currents at the different test pulses were normalized to the current measured at +60 mV at the end of the protocol. The normalized instantaneous currents vs. test pulse voltages were plotted for various $[NaCl]_o$ (Fig. 1E). The reversal potentials (Fig. 1F) were determined from linear fits to the instantaneous I-V relations (solid lines in Fig. 1E). The relative permeabilities estimated by GHK equations (solid lines in Fig. 1F) were $P_{Na} : P_K : P_{Cl} = 1 : 1.14 : 0.52$ and $1 : 1.46 : 0.88$ in the absence or presence 2 mM Ca^{2+}_o, respectively, indicating that CALHM1 is poorly selective with a slight preference for monovalent cations over anions, in agreement with a previous study (3). To extend those studies, we examined the selectivity among monovalent cations. We observed that CALHM1 poorly selects among Group I monovalent cations, with $P_{Na} : P_{Li} : P_K : P_{Rb} : P_{Cs} = 1 : 0.77 : 1.54 : 1.57 : 1.53$ (instantaneous I-V relations in Fig. 1G). Increasing $[Ca^{2+}]_o$ depolarized E_{rev} (Fig. 1H), demonstrating that Ca^{2+} permeates CALHM1. Whereas CALHM1 is

selective for Ca^{2+} over Na^{+}, its selectivity among divalent cations (M^{2+}) is weak, with $P_{Na} : P_{Mg} : P_{Ca} : P_{Ba} = 1 : 3.1 : 13.8 : 8.6$ (Fig. 1I). Taken together, these data indicate that CALHM1 is a poorly selective ion channel.

The CALHM1 Channel Pore Has a Wide Functional Diameter–The relatively poor ion selectivity properties of CALHM1 suggested that its conducting pore might have a wide diameter. To probe the functional diameter of the CALHM1 pore, we examined permeation of various tetraalklylammonium monovalent cations with different sizes (tetramethylammonium (TMA^{+}), tetraethylammonium (TEA^{+}), and tetrabutylammonium (TBA^{+})) (25) (Table 1). Normalized instantaneous I-V relations were used to determine E_{rev} of each tested ion (Fig. 2A), from which the relative permeability of each ion was estimated from an extended constant-field equation (Experimental Procedures *Eqn. 2*) as $P_{Na} : P_{TMA} : P_{TEA} : P_{TBA} = 1 : 0.31 : 0.21 : 0.07$. Thus, CALHM1 has significant permeability to large cations. An exponential relationship between the relative permeability of each amine and its molecular mass (Fig. 2B) suggests that the size of the molecule, rather than binding within the pore, is the major determinant of its permeation (12-14,26). Accordingly, the pore of CALHM1 behaves as a molecular sieve for monovalent cations (12-14,26). By plotting the relative permeabilities against the Pauling radii of the amines, an excluded volume model can be used to estimate the functional diameter of the pore (12-14,26) (Fig. 2C). This method estimates the functional diameter of the CALHM1 pore to be 12.8 Å (Experimental Procedures *Eqn. 6*). A better fit of the data, obtained by adding a term for viscous drag of each ion (red line, Fig. 2C), yielded an estimate of the CALHM1 functional pore diameter of 14.2 Å (Experimental Procedures *Eqn. 7*). Of interest, the relationship between the relative permeabilities of small monovalent cations (from Fig. 1G) and their Stokes radii was also well fitted by the volume-exclusion model that incorporates viscous drag (green triangles, Fig. 2C). These results suggest that small monovalent cations are hydrated when they permeate through the CALHM1 pore. This can account for the lack of ion selectivity observed, and further suggests that the pore is wide.

The estimated functional pore size of CALHM1 is large compared with traditional selective ion channels (3-6 Å) (25-28), whereas it is comparable to those of gap junction-forming connexins (29). The pore properties of connexins have been explored by imaging permeation of fluorescent dyes of different sizes (30,31). As an independent approach to evaluate the CALHM1 functional pore diameter, we measured uptake into CALHM1-expressing neuroblastoma N2a cells of different sized fluorescent molecules with the same electrical valence - Alexa488 (A488), Alexa594 (A594), and Alexa633 (A633), that are structurally related, as well as Lucifer Yellow (LY) (Table 2). Significant uptake of LY, A488, and A594 was observed only in CALHM1 transfected cells and only under conditions in which CALHM1 channels were activated (Fig. 2D). Furthermore, dye uptake was inhibited by a CALHM1 blocker (3) (Ruthenium Red; 20 μM RuR; Fig. 2D), consistent with CALHM1 mediating dye uptake. Uptake of LY and A488 in CALHM1-activated cells was robust, whereas uptake of A594 was less pronounced. A larger molecule, A633, did not permeate in any condition, indicating that its diameter exceeds that of the CALHM1 pore. These results suggest that the diameter of A594 (median axis 13.8 Å) approximates that of the CALHM1 pore. Importantly, this value is in good agreement with the functional pore diameter estimated by electrophysiology (14.2 Å). This independent method of estimating the size of the CALHM1 pore confirms a functional diameter of ~14 Å.

The CALHM1 Channel Pharmacology is Unique–A previous study demonstrated that CALHM1 currents were inhibited by Gd^{3+}, RuR and Zn^{2+}, and partially inhibited by 2-aminoethoxydiphenyl borate (2-APB) (3). Because the pore sizes of CALHM1 are similar to those of connexin and pannexin channels, we asked if the pharmacology of CALHM1 was similar to those channels. We expanded the pharmacological characterization of CALHM1 channels to include probenecid (1 mM), mefloquine (30 μM), and quinine (200 μM), inhibitors of pannexins (32), and specific members of the connexin family (33-35), respectively. None of these compounds inhibited CALHM1 currents (Fig. 1J), indicating that CALHM1 has a

distinct pharmacology compared with connexins and pannexins.

The CALHM1 Ion Channel is a Hexamer–Because the pore sizes of CALHM1 and connexins are similar, we asked if CALHM1 has structural similarities with connexins. Connexin monomers oligomerize to form a hexamer called a connexon (29,36). Whereas CALHM1 was previously suggested to oligomerize to form tetramers (1,2), we re-investigated the oligomeric status of CALHM1 in transiently-transfected mouse Neuro-2a (N2a) cells, first using SDS-PAGE. Under non-reducing conditions, two bands were present: one at ~80 kDa and another ~250 kDa, corresponding to ~two and six times the mass of a CALHM1 monomer. Both bands disappeared upon the addition of the reducing agent β-mercaptoethanol (βME), with a single band at 40 kDa (Fig. 3A), the expected mass of monomeric CALHM1, becoming dominant. To obtain another estimation of the oligomeric mass of CALHM1, Blue Native polyacrylamide gel electrophoresis (BN-PAGE) was employed (37,38). One CALHM1 immunoreactive band was observed at ~240 kDa under non-reducing conditions specifically in cells transfected with CALHM1 (Fig. 3B), similar to the molecular weight of the band observed in non-reducing SDS-PAGE. Since a CALHM1 monomer has molecular mass ~ 40 kDa, these results suggest that CALHM1 might be larger than a tetramer, perhaps a hexamer.

A caveat of BN-PAGE or non-reducing SDS-PAGE for determination of molecular stoichiometry is that the protein might be associated with other proteins that contribute to the observed mass. We therefore used single-molecule subunit counting (21) to determine the number of monomers that form a CALHM1 channel. CALHM1-EGFP was expressed in *Xenopus* oocytes and imaged at the plasma membrane using total internal reflection fluorescence (TIRF) microscopy (Fig. 3C). Expression of carboxyl-terminal EGFP-tagged CALHM1 generated ionic currents similar to untagged CALHM1 (not shown). The fluorescence intensities of immobile fluorescent particles were measured over time. Only particles that bleached completely and displayed at least one discrete bleaching step were analyzed (as in Fig. 3D). Using the StepFinder algorithm (17) to objectively determine the number of bleaching steps, most of the immobile fluorescent spots bleached in 5 steps, with a significant fraction bleaching in 6 steps (Fig. 3E). None of the particles bleached in more than 6 steps. Since not every EGFP molecule is fluorescent (18,21-23,39), the distribution of bleaching steps follows a binomial distribution with a probability (p) of EGFP being fluorescent. The data were best fitted by a binomial distribution assuming a 6-mer, with p = 74.6% (Fig. 3E; Experimental Procedures *Eqn 8*), similar to previous studies that determined ~80% of EGFP molecules are fluorescent (21,23,39). Visual inspection analysis (15,18,22,23) revealed a similar distribution, with the data well fitted by a binomial distribution assuming a 6-mer, with p = 80.2% (Fig. 3F; Experimental Procedures *Eqn* 8). These results indicate that a CALHM1 channel is a hexamer of CALHM1 monomers, consistent with the conclusion reached from the SDS- and BN-PAGE determinations.

CALHM1 has Four Transmembrane Helices with Cytoplasmic Termini–These results indicate that a CALHM1 ion channel is a hexamer with a large pore diameter. These structural features are similar to those of gap-junction forming connexons. We asked whether structural similarities between CALHM1 and connexons extended to the secondary structures of their monomers. Connexins have 4 membrane spanning helices (TM) (29,36). Although CALHM1 was originally proposed to have three TM and one re-entrant hydrophobic loop (1), TM-prediction algorithms (40-45) suggest that human CALHM1 and other CALHMs have 3 to 6 hydrophobic domains (Fig. 4A), with the majority predicting four TM with cytoplasmic amino- and carboxyl-termini (Fig. 4B). Three prediction programs propose an additional TM domain between residues 123 and 150. This stretch of residues contains a putative N-glycosylation site, Asn140. N-glycosylation of this residue would indicate that this region is not in a TM domain but is instead located in an extracellular loop in the protein. We therefore confirmed that Asn140 is N-glycosylated (1) (Fig. 4C), indicating that this region is not a TM but is part of an extracellular loop between TM3 and TM4. We determined the localization of the CALHM1 carboxyl-terminus by exposing

permeabilized or non-permeabilized transiently-transfected PC12 cells to an antibody directed against the CALHM1 carboxyl-terminus. CALHM1 was detected only in cells exposed to the permeabilized immunostaining protocol (Fig. 4D), suggesting that the carboxyl-terminus is located in the cytoplasm. These results are consistent with a CALHM1 topology of four TM with cytoplasmic amino- and carboxyl-termini (Fig. 4B), similar to connexins.

CALHM1 Does Not Form Gap Junctions– The structural similarities between CALHM1 and connexins suggest the two proteins may have a similar functions. We asked if CALHM1 can form gap junctions in a manner similar to connexons. The ability of CALHM1 or connexin 30 (Cx30) to form gap junctions was tested by using a microelectrode back-filled with Alexa350 dye (Table 2) to fill one transfected cell in a cluster of transfected cells with dye, and measuring the extent of dye transfer to other cells in the cluster (Fig. 5A). 9 of 11 (81.8 %) Cx30-transfected dye-loaded cells transferred dye to at least one other cell. Furthermore, Cx30 dye-loaded cells transferred dye to 2.4 ± 0.6 other cells. These results confirm that Cx30 forms gap junctions (46). In contrast, only 1 of 12 (8.3 %) dye-loaded CALHM1-transfected cells transferred dye to another cell, similar to dye-loaded GFP-transfected cells (Fig. 5B). The lone CALHM1-transfected cell that did transfer dye transferred it to only one other cell (Fig. 5C). We considered that CALHM1 might form gap junctions but that the presence of extracellular Ca^{2+} in these experiments kept CALHM1 closed, preventing dye transfer. To test this, experiments were also performed in the absence of extracellular Ca^{2+}. CALHM1 activation by low $[Ca^{2+}]_o$ (3) resulted in dye leakage through CALHM1 to the extracellular space, but no dye transfer to adjacent CALHM1-expressing cells was observed (data not shown). These data, together with the observation that Asp140 is N-glycosylated, strongly suggest that CALHM1 does not form gap junctions, but instead functions as an unapposed plasma membrane ion channel (3).

DISCUSSION

The present study is the first structural investigation of the CALHM1 ion channel. Based on our results, we conclude that CALHM1 has four transmembrane domains with a cytoplasmic amino- and carboxyl-termini, and that it forms a hexameric, nonselective ion channel with a wide permeation pore. The structural characteristics of CALHM1 are similar to those of connexins, pannexins, and innexins. However, unlike connexins and innexins, CALHM1 does not form gap junctions.

The Permeation Pathway of CALHM1. Our electrophysiological analyses of mono- and divalent cation permeation indicate that CALHM1 forms a nonselective ion channel with only weak charge selectivity, with $P_{divalent\ cation} > P_{monovalent\ cation} > P_{monovalent\ anion}$. Of note, the selectivity sequence of CALHM1 is remarkably similar to that of connexins rCx40 and rCx43 (47) and rCx43 (48).

Two independent methods demonstrated that the pore of CALHM1 has a ~7 Å functional radius at its narrowest region (Fig. 2). In the first method, the relative permeabilities of various tetraalkylammonium ions were determined and then used to estimate the functional pore radius. These ions have similar shapes and valence, differing only in their radii. Fitting the data with a volume exclusion model estimated a functional pore radius of ~7 Å. Although the parabolic dependence of the volume exclusion model predicts that molecules larger than 7.1 Å would permeate CALHM1, this behavior was not observed. Notably, this model is also able to predict the relative permeabilities of the Group I monovalent cations examined (Fig. 1G) when plotted versus their respective Stokes' radii. The Stokes' radius accounts for the hydration but not the shape of the ion, which could lead to an underestimation of the true radius of the ions since most ions are not perfectly spherical.

These results suggest that small ions remain at least partially hydrated as they permeate the pore. The hydration shell can shield the ion from the amino acids that line the pore, minimizing interactions that could promote selectivity. Larger ions that approach the size of the pore may be able to interact with the pore lining residues, resulting in increased selectivity among big ions.

In the second method, we employed optical imaging of fluorescent dye uptake using dyes of the same valence and similar structure with different sizes. The smallest dyes, LY and A488

(Table 2), easily permeated through CALHM1. The influx of A594 was significantly less robust, suggesting that the dimensions of A594 (median axis 13.8 Å) approach the diameter of the pore. The largest dye, A633, did not permeate through CALHM1. Structural information about A633 is unavailable because it is considered proprietary by its manufacturer. Conversations with representatives of the manufacturer revealed that its structure is similar to those of the other Alexa dyes with a mass ~1150 g/mol. Assuming that the larger mass is correlated with an increase in its molecular dimensions, it is reasonable to conclude that the diameter of A633 is > 13.8 Å. These results also suggest that the CALHM1 functional pore diameter ~ 14 Å.

The good agreement between two independent experimental approaches suggests that the CALHM1 functional pore diameter is ~ 14.2 Å. The CALHM1 pore is therefore quite large compared with most ion channels, e.g. nicotinic receptors (9.2 Å; (12,49)), voltage-gated Ca^{2+} channels (6 Å; (26)), NMDA receptors (7.2 Å; (50)), Orai1 (3.8 Å; (51)), Orai3 (3.8Å; (52)), voltage-gated K^+ channels (4.7 Å; (53)), voltage-gated Na^+ channels (6.1 Å; (25)), and cyclic nucleotide-gated channels (9.2 Å; (54)). The pore diameter of CALHM1 is comparable to those of connexons (Cx26 (14 Å; (29)), Cx43 (12.6 Å; (48)), Cx40 (13.2 Å; (47)), Cx32 (between 12 and 14 Å; (55)) whereas it is smaller than those of Panx1 and Panx2 (17-21 Å and 30 Å, respectively (56)).

While the pore radius of CALHM1 is large, its unitary monovalent cation conductance is only 24 pS (3). The unitary conductances of connexon channels are not highly correlated with their pore diameters (reviewed in (57)). Lack of correlation between the pore diameter and unitary conductance can occur if the narrowest region of a wide pore extends for a relatively long distance. An ion traversing the pore would be able to interact with multiple sites in the pore, retarding its diffusion and reducing its conductance.

The CALHM1 Ion Channel is a Hexamer. CALHM1 was previously shown to homo-oligomerize (1). In the previous study, only monomeric CALHM1 (~40 kDa) was observed under reducing conditions, whereas ~160 and 80 kDa immunoreactive bands were observed in under non-reducing conditions (1), consistent with the proposal that CALHM1 can form tetramers and dimers, respectively. We noted that the gel employed previously spanned a limited range of protein mass, 70 to ~150 kDa, which could preclude detection of possible oligomers larger than a tetramer. To determine if CALHM1 can form complexes larger than 160 kDa, we repeated SDS-PAGE experiments using gels that span a wider range of molecular mass (Fig. 3A). In the absence of βME, we observed prominent bands ~250 kDa and ~80 kD, suggesting that CALHM1 can form oligomers larger than a tetramer. In the presence of βME, the intensity of the higher molecular weight band diminished and a single prominent band at ~40 kDa appeared. Accordingly, SDS and boiling alone are insufficient to denature the CALHM1 complex. Instead, reducing agents must be used to denature the CALHM1 complex. In the absence of a reducing agent, the molecular mass markers may slightly overestimate the molecular mass of the CALHM1 complex because the markers are denatured proteins that likely migrate faster than non-denatured, non-reduced CALHM1 complex. Thus, the observed ~250 kD band is consistent with the expected 240 kD mass of a CALHM1 hexamer.

Another estimate of the mass of the CALHM1 complex was obtained using BN-PAGE (Fig. 3B). BN-PAGE uses Coomassie® G-250 as a charge-shift molecule instead of SDS, enabling proteins to remain in their native conformations as they migrate through the gel. In the absence of βME, a single CALHM1 band was present at ~240 kDa. This is a more accurate estimation because the molecular mass markers are also in their native conformations. Despite repeated attempts with a range of concentrations, we were unable to detect lower molecular weight CALHM1 species when the sample was reduced by βME. The inability to detect even monomeric CALHM1 is likely because denatured CALHM1 migrates rapidly through the BN-PAGE gel. Nevertheless, the detection of a ~250 kD species by both non-reducing SDS-PAGE and non-denaturing BN-PAGE suggests that native CALHM1 is likely composed of greater than 4, possibly 6, CALHM1 monomers.

The major caveat of non-reducing SDS-PAGE as well as BN-PAGE is that other proteins can contribute mass to the CALHM1 complex. Thus, a complex with mass of ~240 kDa does not necessarily imply that it contains six CALHM1 monomers. Furthermore, proteins with native conformations with acidic isoelectric points and compact structures may migrate faster than other proteins in non-reducing PAGE, introducing errors up to 15% in the mass estimation (37).

Since many factors including size, charge, and shape of the protein determine how quickly it migrates through a gel, we employed an alternate approach to determine the subunit stoichiometry of a CALHM1 channel. Single-molecule photobleaching experiments were used to determine the number of CALHM1 monomers in a functional CALHM1 ion channel complex. This method takes advantage of the discrete nature of GFP photobleaching to directly determine the number of subunits in membrane proteins by counting the bleaching steps of single fluorescent proteins (21). Since CALHM1 is genetically fused to GFP, the number of bleaching steps represents the number of GFP-tagged subunits in the complex. This technique has been used previously to determine the stoichiometry of membrane proteins that have up to seven monomers in the complex (58). The low expression level of the protein reduced the probability of aggregation of multiple complexes in the same pixel region.

Consistent with the photobleaching traces shown in Fig. 3D, previous reports have shown that the amplitude of successive bleaching steps recorded from mulitmeric-tagged proteins can vary (18-21). There are four main reasons for this behavior (19). First, the orientation of different fluorophores, even in the same complex, is different. Second, fluorophores with the same orientation can interact with various surface impurities or charges, which can lead to variability in fluorescence emission intensity. Third, the location of the oligomer relative to the focus of the excitation laser beam can produce different fluorescence intensities. Finally, since we employed a TIRF microscope, the fluorophore's distance into the cell can alter its fluorescence emission intensity. Therefore, the number of bleaching steps cannot be determined by dividing the total fluorescence intensity by the intensity of a single bleaching step. As a result, we are not able to detect multiple bleaching steps if they photobleach simultaneously.

Using both StepFinder and visual inspection to identify photobleaching steps, the highest percentage of particles bleached in five steps, with a significant percentage bleaching in six steps. The distribution of CALHM1-EGFP bleaching steps should approximate a binomial distribution with two parameters: total number of molecules in the complex and the percentage of EGFP molecules that initially fluoresce. Fitting the data with a binomial equation that assumed the total number of molecules in the complex but allowed the percent of fluorescing EGFP molecules to be free, the StepFinder distribution was fitted best assuming a 6mer with 74.6% of the GFP molecules initially fluorescent. By visual inspection, the distribution of bleaching steps was fitted well by a 6mer with 80.2% of the GFP molecules fluorescent. Previous similar experiments (21,23,39) found that ~20% of the GFPs are in a non-fluorescing state, possibly due to misfolding or incomplete maturation of the GFP. Our determinations are in good agreement with those results, which is perhaps not unexpected since we used the same fluorophore from the same source as those studies (EGFP from Clontech's pEGFP-N1). Accordingly, the distribution of bleaching steps can be fitted best assuming that CALHM1 is a hexamer.

The two methods used to identify bleaching steps had similar results. The visual inspection method identified some very fast bleaching steps that StepFinder did not identify, because the magnitude of the bleaching steps was less than the noise of the measurement, causing a right-shift of the distribution of bleaching steps. The visual inspection method also identified a small percentage of particles that bleached in > 6 steps, likely due to more than one CALHM1 complex being in the same pixel region.

The Structure of CALHM1 is Similar to Those of Connexins and Pannexins/Innexins. Connexins comprise a large family of gap junction proteins in vertebrates (59,60). Functional studies have identified innexins as the proteins responsible for forming functional hemichannels and gap junctions in invertebrates (61-64). However, innexins and connexins have no evolutionary relationship (59,61,62,65,66). In contrast,

pannexins are vertebrate homologs of innexins (59,67,68), but they do not form gap junctions, functioning instead as unapposed plasma membrane ion channels (69). Connexons (29,36) and pannexins (Panx1 (70)) are hexameric assemblies of subunits. The amino acid sequences of Panx1 and Cx43, which have no evolutionary relationship, are 18.7% similar. By the same analysis, the CALHM1 amino acid sequence is 18.3% and 17.9% similar to Panx1 and Cx43, respectively, suggesting that CALHM1 shares no evolutionary relationship with these or other protein families (71,72). Nevertheless, like connexons (29,36) and Panx1 (70), the CALHM1 ion channel is comprised of a hexamer of subunits that surround a wide central pore. Furthermore, we note that CALHMs, connexins and innexins/pannexins share secondary structural features (73) (Fig. 6). In addition to the presence of four TM domains, all three families possess an amino-terminal α-helix, a ß-sheet in the second extracellular loop, and, except for connexins, α-helical regions in the carboxyl-termini, that align well (Fig. 4E). Conserved cysteines in the two extracellular loops are present in all three families. Connexins have 3 conserved Cys residues in each extracellular loop, pannexins and innexins have 2 Cys in each loop (74,75) and CALHM proteins also have 2 conserved Cys in the first extracellular loop, and while there are multiple Cys in the second extracellular loop, only two are conserved among all members of the CALHM family. Pannexins and CALHMs are distinguished from the gap junction-forming connexins and innexins by being N-glycosylated (76), a post-translational modification that when introduced into connexins prevents gap junction formation (Cx32, (77,78)), and when removed from Panx1 increases junctional conductance in paired oocytes expressing (77). CALHM1 does not appear to form gap junctions (Fig. 5), but instead it functions as an unapposed plasma membrane ion channel (3).

CALHM1, connexins and pannexins/innexins have similar structural features that confer both shared and distinct functional properties. Like connexons (79-81) and pannexin channels (74,82-85), CALHM1 is activated by membrane depolarization (3), although their kinetic responses are distinct. Reduced $[Ca^{2+}]_o$ activates connexons (79-81) and CALHM1 (3) but not pannexins (83). Pannexins and connexins share pharmacological features that are absent in CALHM1 (3,83,86) (Fig. 1J). The predominant function of connexins is to form gap junctions that allow the passage of molecules up to 1 kD between cells. Plasma membrane hemi-channels exist, although their physiological roles are not clear. Pannexins and connexons have been proposed to mediate cellular release of large molecules, including adenine nucleotides and prostaglandins, that could act as autocrine and paracrine signaling factors (57,82,87,88). The similar structural features of CALHM1 suggest that in addition to acting as a sensor of extracellular Ca^{2+} in the brain (3), it may also participate in similar signaling functions. While sequence analysis suggests that CALHMs, connexins and pannexins share no evolutionary relationship, the structural and functional similarities of CALHM1 with connexin, pannexin, and innexin protein families defines CALHM as a new family within a super-family of proteins related by structural homoplasy that have shared and distinct functional properties and roles in cellular physiology.

REFERENCES

1. Dreses-Werringloer, U., Lambert, J. C., Vingtdeux, V., Zhao, H., Vais, H., Siebert, A., Jain, A., Koppel, J., Rovelet-Lecrux, A., Hannequin, D., Pasquier, F., Galimberti, D., Scarpini, E., Mann, D., Lendon, C., Campion, D., Amouyel, P., Davies, P., Foskett, J. K., Campagne, F., and Marambaud, P. (2008) *Cell* **133**, 1149-1161
2. Lambert, J. C., and Amouyel, P. (2007) *Psychoneuroendocrinology* **32 Suppl 1**, S62-70
3. Ma, Z., Siebert, A. P., Cheung, K. H., Lee, R. J., Johnson, B., Cohen, A. S., Vingtdeux, V., Marambaud, P., and Foskett, J. K. (2012) *Proc Natl Acad Sci U S A* **109**, E1963-1971
4. Gallego-Sandin, S., Alonso, M. T., and Garcia-Sancho, J. (2011) *Biochem J* **437**, 469-475
5. Moreno-Ortega, A. J., Ruiz-Nuno, A., Garcia, A. G., and Cano-Abad, M. F. *Biochem Biophys Res Commun* **391**, 722-726

6. Bahima, L., Aleu, J., Elias, M., Martin-Satue, M., Muhaisen, A., Blasi, J., Marsal, J., and Solsona, C. (2006) *J Cell Physiol* **206**, 95-102
7. Ebihara, L. (1996) *Biophys J* **71**, 742-748
8. Weber, W. (1999) *Biochim Biophys Acta* **1421**, 213-233
9. Hille, B. (2001) *Ion channels of excitable membranes*, 3rd ed., Sinauer, Sunderland, Mass.
10. Wu, W. J. H. a. Y.-C. (1972) *Journal of Physical and Chemical Reference Data* **1**, 1047-1099
11. Adams, D. J., Dwyer, T. M., and Hille, B. (1980) *J Gen Physiol* **75**, 493-510
12. Dwyer, T. M., Adams, D. J., and Hille, B. (1980) *J Gen Physiol* **75**, 469-492
13. Farris, H. E., LeBlanc, C. L., Goswami, J., and Ricci, A. J. (2004) *J Physiol* **558**, 769-792
14. Sun, Y. M., Favre, I., Schild, L., and Moczydlowski, E. (1997) *J Gen Physiol* **110**, 693-715
15. Penna, A., Demuro, A., Yeromin, A. V., Zhang, S. L., Safrina, O., Parker, I., and Cahalan, M. D. (2008) *Nature* **456**, 116-120
16. Demuro, A., and Parker, I. (2005) *J Biomed Opt* **10**, 11002
17. Kerssemakers, J. W., Munteanu, E. L., Laan, L., Noetzel, T. L., Janson, M. E., and Dogterom, M. (2006) *Nature* **442**, 709-712
18. Demuro, A., Penna, A., Safrina, O., Yeromin, A. V., Amcheslavsky, A., Cahalan, M. D., and Parker, I. (2011) *Proc Natl Acad Sci U S A* **108**, 17832-17837
19. Ding, H., Wong, P. T., Lee, E. L., Gafni, A., and Steel, D. G. (2009) *Biophys J* **97**, 912-921
20. Ji, W., Xu, P., Li, Z., Lu, J., Liu, L., Zhan, Y., Chen, Y., Hille, B., Xu, T., and Chen, L. (2008) *Proc Natl Acad Sci U S A* **105**, 13668-13673
21. Ulbrich, M. H., and Isacoff, E. Y. (2007) *Nat Methods* **4**, 319-321
22. Nakajo, K., Ulbrich, M. H., Kubo, Y., and Isacoff, E. Y. (2010) *Proc Natl Acad Sci U S A* **107**, 18862-18867
23. Yu, Y., Ulbrich, M. H., Li, M. H., Buraei, Z., Chen, X. Z., Ong, A. C., Tong, L., Isacoff, E. Y., and Yang, J. (2009) *Proc Natl Acad Sci U S A* **106**, 11558-11563
24. Sitaram, A., Piccirillo, R., Palmisano, I., Harper, D. C., Dell'Angelica, E. C., Schiaffino, M. V., and Marks, M. S. (2009) *Mol Biol Cell* **20**, 1464-1477
25. Hille, B. (1971) *J Gen Physiol* **58**, 599-619
26. McCleskey, E. W., and Almers, W. (1985) *Proc Natl Acad Sci U S A* **82**, 7149-7153
27. Meuser, D., Splitt, H., Wagner, R., and Schrempf, H. (1999) *FEBS Lett* **462**, 447-452
28. Nishida, M., and MacKinnon, R. (2002) *Cell* **111**, 957-965
29. Maeda, S., Nakagawa, S., Suga, M., Yamashita, E., Oshima, A., Fujiyoshi, Y., and Tsukihara, T. (2009) *Nature* **458**, 597-602
30. Weber, P. A., Chang, H. C., Spaeth, K. E., Nitsche, J. M., and Nicholson, B. J. (2004) *Biophys J* **87**, 958-973
31. Elfgang, C., Eckert, R., Lichtenberg-Frate, H., Butterweck, A., Traub, O., Klein, R. A., Hulser, D. F., and Willecke, K. (1995) *J Cell Biol* **129**, 805-817
32. Silverman, W., Locovei, S., and Dahl, G. (2008) *Am J Physiol Cell Physiol* **295**, C761-767
33. Cruikshank, S. J., Hopperstad, M., Younger, M., Connors, B. W., Spray, D. C., and Srinivas, M. (2004) *Proc Natl Acad Sci U S A* **101**, 12364-12369
34. Martinez-Wittinghan, F. J., Srinivas, M., Sellitto, C., White, T. W., and Mathias, R. T. (2006) *J Membr Biol* **211**, 163-171
35. Srinivas, M., Hopperstad, M. G., and Spray, D. C. (2001) *Proc Natl Acad Sci U S A* **98**, 10942-10947
36. Maeda, S., and Tsukihara, T. (2011) *Cell Mol Life Sci* **68**, 1115-1129
37. Schagger, H., Cramer, W. A., and von Jagow, G. (1994) *Anal Biochem* **217**, 220-230
38. Schagger, H., and von Jagow, G. (1991) *Anal Biochem* **199**, 223-231
39. Tombola, F., Ulbrich, M. H., and Isacoff, E. Y. (2008) *Neuron* **58**, 546-556
40. Claros, M. G., and von Heijne, G. (1994) *Comput Appl Biosci* **10**, 685-686
41. Krogh, A., Larsson, B., von Heijne, G., and Sonnhammer, E. L. (2001) *J Mol Biol* **305**, 567-580
42. Rost, B., Fariselli, P., and Casadio, R. (1996) *Protein Sci* **5**, 1704-1718

43. Sonnhammer, E. L., von Heijne, G., and Krogh, A. (1998) *Proc Int Conf Intell Syst Mol Biol* **6**, 175-182
44. Tusnady, G. E., and Simon, I. (2001) *Bioinformatics* **17**, 849-850
45. von Heijne, G. (1992) *J Mol Biol* **225**, 487-494
46. Common, J. E., Becker, D., Di, W. L., Leigh, I. M., O'Toole, E. A., and Kelsell, D. P. (2002) *Biochem Biophys Res Commun* **298**, 651-656
47. Beblo, D. A., and Veenstra, R. D. (1997) *J Gen Physiol* **109**, 509-522
48. Wang, H. Z., and Veenstra, R. D. (1997) *J Gen Physiol* **109**, 491-507
49. Dani, J. A. (1989) *J Neurosci* **9**, 884-892
50. Zarei, M. M., and Dani, J. A. (1995) *J Neurosci* **15**, 1446-1454
51. Yamashita, M., Navarro-Borelly, L., McNally, B. A., and Prakriya, M. (2007) *J Gen Physiol* **130**, 525-540
52. Schindl, R., Bergsmann, J., Frischauf, I., Derler, I., Fahrner, M., Muik, M., Fritsch, R., Groschner, K., and Romanin, C. (2008) *J Biol Chem* **283**, 20261-20267
53. Bezanilla, F., and Armstrong, C. M. (1972) *J Gen Physiol* **60**, 588-608
54. Balasubramanian, S., Lynch, J. W., and Barry, P. H. (1995) *J Membr Biol* **146**, 177-191
55. Oh, S., Ri, Y., Bennett, M. V., Trexler, E. B., Verselis, V. K., and Bargiello, T. A. (1997) *Neuron* **19**, 927-938
56. Ambrosi, C., Gassmann, O., Pranskevich, J. N., Boassa, D., Smock, A., Wang, J., Dahl, G., Steinem, C., and Sosinsky, G. E. (2010) *J Biol Chem* **285**, 24420-24431
57. Harris, A. L. (2007) *Prog Biophys Mol Biol* **94**, 120-143
58. Das, S. K., Darshi, M., Cheley, S., Wallace, M. I., and Bayley, H. (2007) *Chembiochem* **8**, 994-999
59. Panchin, Y., Kelmanson, I., Matz, M., Lukyanov, K., Usman, N., and Lukyanov, S. (2000) *Curr Biol* **10**, R473-474
60. Fushiki, D., Hamada, Y., Yoshimura, R., and Endo, Y. (2010) *Biomed Res* **31**, 133-142
61. Phelan, P., Bacon, J. P., Davies, J. A., Stebbings, L. A., Todman, M. G., Avery, L., Baines, R. A., Barnes, T. M., Ford, C., Hekimi, S., Lee, R., Shaw, J. E., Starich, T. A., Curtin, K. D., Sun, Y. A., and Wyman, R. J. (1998) *Trends Genet* **14**, 348-349
62. Barnes, T. M. (1994) *Trends Genet* **10**, 303-305
63. Starich, T. A., Lee, R. Y., Panzarella, C., Avery, L., and Shaw, J. E. (1996) *J Cell Biol* **134**, 537-548
64. Landesman, Y., White, T. W., Starich, T. A., Shaw, J. E., Goodenough, D. A., and Paul, D. L. (1999) *J Cell Sci* **112 (Pt 14)**, 2391-2396
65. Bruzzone, R., White, T. W., and Paul, D. L. (1996) *Eur J Biochem* **238**, 1-27
66. White, T. W., Deans, M. R., O'Brien, J., Al-Ubaidi, M. R., Goodenough, D. A., Ripps, H., and Bruzzone, R. (1999) *Eur J Neurosci* **11**, 1883-1890
67. Baranova, A., Ivanov, D., Petrash, N., Pestova, A., Skoblov, M., Kelmanson, I., Shagin, D., Nazarenko, S., Geraymovych, E., Litvin, O., Tiunova, A., Born, T. L., Usman, N., Staroverov, D., Lukyanov, S., and Panchin, Y. (2004) *Genomics* **83**, 706-716
68. Yen, M. R., and Saier, M. H., Jr. (2007) *Prog Biophys Mol Biol* **94**, 5-14
69. Sosinsky, G. E., Boassa, D., Dermietzel, R., Duffy, H. S., Laird, D. W., MacVicar, B., Naus, C. C., Penuela, S., Scemes, E., Spray, D. C., Thompson, R. J., Zhao, H. B., and Dahl, G. (2011) *Channels (Austin)* **5**, 193-197
70. Boassa, D., Ambrosi, C., Qiu, F., Dahl, G., Gaietta, G., and Sosinsky, G. (2007) *J Biol Chem* **282**, 31733-31743
71. Larkin, M. A., Blackshields, G., Brown, N. P., Chenna, R., McGettigan, P. A., McWilliam, H., Valentin, F., Wallace, I. M., Wilm, A., Lopez, R., Thompson, J. D., Gibson, T. J., and Higgins, D. G. (2007) *Bioinformatics* **23**, 2947-2948
72. Goujon, M., McWilliam, H., Li, W., Valentin, F., Squizzato, S., Paern, J., and Lopez, R. (2010) *Nucleic Acids Res* **38**, W695-699

73. Pei, J., and Grishin, N. V. (2007) *Bioinformatics* **23**, 802-808
74. Barbe, M. T., Monyer, H., and Bruzzone, R. (2006) *Physiology (Bethesda)* **21**, 103-114
75. Hua, V. B., Chang, A. B., Tchieu, J. H., Kumar, N. M., Nielsen, P. A., and Saier, M. H., Jr. (2003) *J Membr Biol* **194**, 59-76
76. Penuela, S., Bhalla, R., Gong, X. Q., Cowan, K. N., Celetti, S. J., Cowan, B. J., Bai, D., Shao, Q., and Laird, D. W. (2007) *J Cell Sci* **120**, 3772-3783
77. Boassa, D., Qiu, F., Dahl, G., and Sosinsky, G. (2008) *Cell Commun Adhes* **15**, 119-132
78. Dahl, G., Nonner, W., and Werner, R. (1994) *Biophys J* **67**, 1816-1822
79. Srinivas, M., Calderon, D. P., Kronengold, J., and Verselis, V. K. (2006) *J Gen Physiol* **127**, 67-75
80. Verselis, V. K., and Srinivas, M. (2008) *J Gen Physiol* **132**, 315-327
81. Ebihara, L. (2003) *News Physiol Sci* **18**, 100-103
82. Bao, L., Locovei, S., and Dahl, G. (2004) *FEBS Lett* **572**, 65-68
83. Bruzzone, R., Barbe, M. T., Jakob, N. J., and Monyer, H. (2005) *J Neurochem* **92**, 1033-1043
84. Bruzzone, R., Hormuzdi, S. G., Barbe, M. T., Herb, A., and Monyer, H. (2003) *Proc Natl Acad Sci U S A* **100**, 13644-13649
85. Locovei, S., Wang, J., and Dahl, G. (2006) *FEBS Lett* **580**, 239-244
86. Eskandari, S., Zampighi, G. A., Leung, D. W., Wright, E. M., and Loo, D. D. (2002) *J Membr Biol* **185**, 93-102
87. Qiu, F., and Dahl, G. (2009) *Am J Physiol Cell Physiol* **296**, C250-255
88. Shestopalov, V. I., and Panchin, Y. (2008) *Cell Mol Life Sci* **65**, 376-394
89. Veenstra, R. D., Wang, H. Z., Beyer, E. C., Ramanan, S. V., and Brink, P. R. (1994) *Biophys J* **66**, 1915-1928
90. Nightingale, E. R. (1959) *The Journal of Physical Chemistry* **63**, 1381-1387

Acknowledgments–We thank Drs. M. S. Marks and A. Sitaram for the 3xHA-OCA2 plasmid; Dr. P. Marambaud for the CALHM1 antibody; Dr. S. W. Yum for the Cx30 plasmid; Drs. Y. E. Goldman and Y. Sun for help with preliminary photo-bleaching studies; Drs. N. A. Cohen and R. J. Lee for use of their microscope; and Drs. C. Deutsch, T. Hoshi, B. Salzberg, D. Ren, S. Baylor, H. Vais, D. D.-O. Mak, and Ms. Marioly Muller for helpful discussions. This work was supported by funds from the NIH to JKF (MH059937 and GM056328) and to IP (GM048071).

AUTHOR CONTRIBUTIONS

A.P.S., Z.M., J.D.G., and A.D. performed the experiments. A.P.S., Z.M., I.P. and J.K.F. designed the experiments. A.P.S. and J.K.F wrote the manuscript.

COMPETING FINANCIAL INTERESTS

The authors declare no competing financial interests.

FIGURE LEGENDS

FIGURE 1. CALHM1 is a poorly selective ion channel. (A) Divalent-Free Voltage Protocol. (B) Divalent Voltage Protocol. (C) Representative families of current traces from CALHM1-expressing (red) and control (blue) oocytes in response to the Divalent-Free Voltage Protocol shown in *Panel A* and

described in *Experimental Procedures*. Oocytes were bathed in a solution containing (in mM): 100 NaCl, 10 HEPES, 0.5 EGTA, 0.5 EDTA, pH 7.3. (D) Representative families of current traces from CALHM1-expressing (red) and control (blue) oocytes in response to the Divalent Voltage Protocol shown in *Panel B* and described in the *Experimental Procedures*. Oocytes were bathed in a solution containing (in mM): 100 NaCl, 2 $CaCl_2$, 10 HEPES, pH 7.3. (E) Normalized instantaneous current-voltage (I-V) curves from representative CALHM1-expressing oocyte. Increasing $[NaCl]_o$ depolarized E_{rev}. The solid lines are linear fits. (F) Permeabilities of K^+, Cl^-, and Ca^{2+} relative to Na^+ were determined by plotting E_{rev} from (E) versus $[NaCl]_o$ in the absence (red) or presence (black) of $Ca^{2+}{}_o$ and the solid lines were calculated by fitting the data with either the GHK constant field equation (*Eqn 1*) or the extended constant field equation (*Eqn 2*), respectively. (G) Normalized instantaneous I-V curves from representative CALHM1-expressing oocytes bathed in 100 mM monovalent cation solutions. Shifts in E_{rev} enabled calculation of relative permeabilities. Solid lines are linear fits. (H) Normalized instantaneous I-V curves from representative CALHM1-expressing oocytes bathed in various $[Ca^{2+}]_o$. Increasing $[Ca^{2+}]_o$ depolarized E_{rev}. Solid lines are linear fits. (I) Relative permeabilities of divalent cations (M^{2+}) were determined by plotting E_{rev} from (H) versus bath M^{2+} activity and the solid lines were derived from fitting the data with the constant field equation (*Eqn 2*). (J) Pharmacology of CALHM1 currents. Averaged, normalized currents (mean ± s.e.m.) are shown for 1 mM probenecid (green, n=4), 30 μM mefloquine (red, n=4) and 200 μM quinine (blue, n=4). Black line represents currents recorded in control oocyte injected only with Cx38 antisense oligonucleotide, normalized to the average CALHM1 currents (7.8 ± 1.1 μA, n=12) from the same batch of oocytes.

FIGURE 2. The ion-conducting pore of CALHM1 is wide. (A) Normalized instantaneous I-V curves of representative CALHM1-expressing oocytes bathed in various sized tetraalkylammonium cations (Table 2) using the Divalent Free Voltage Protocol (Fig. 1A). Solid lines are linear fits, error bars indicate ± s.e.m. (B) Plot of relative permeability of each cation against its molecular mass is an exponential relationship. (C) Plot of relative permeability of each cation versus its respective ionic radius. Fitting data with Volume-Exclusion equation (blue curve; Experimental Procedures *Eqn 6*) estimates a pore diameter of 12.8 Å. Fitting data with Volume Exclusion equation including a term for the viscous drag of the ion (red curve; Experimental Procedures *Eqn 7*) estimates a pore diameter of 14.2Å. Relative permeabilities of monovalent cations from Fig. 1G plotted versus their Stokes' radii (green triangles). (D) *Left:* Box plots of fluorescence intensities of intracellular Lucifer Yellow, Alexa488, Alexa594, and Alexa633 taken up by mock- and CALHM1-transfected cells in the presence (5 mM) or absence of extracellular Ca^{2+} to inhibit or activate CALHM1 opening, respectively. Data plotted on log scale. Numbers of cells for each condition ranged from 316 to 1489. For each box plot, middle line represents median; upper and lower bounds of box represent 75^{th} and 25^{th} percentiles, respectively; and upper and lower tails represent 90^{th} and 10^{th} percentiles, respectively. For each dye, median fluorescence intensities were compared between transfection conditions and extracellular calcium conditions only, using the Kruskal-Wallis test. Therefore, statistical significance was adjusted to correct for multiple comparisons; ° = $p < 0.01$ and * = $p < 0.0125$. Cells not expressing CALHM1 and cells incubated in solutions containing 5 mM Ca^{2+} showed background levels of fluorescence. *Right:* Representative fluorescence images in dye uptake experiments. Regions of interest (blue traces) were drawn around morphologically normal cells in each field. *Left Panel:* Mock-transfected cells incubated in solutions containing 0 Ca^{2+}. *Middle Panel:* CALHM1-transfected cells incubated in solutions containing 5 mM Ca^{2+}. *Right Panel:* CALHM1-transfected cells incubated in solutions containing 0 Ca^{2+}.

FIGURE 3. CALHM1 channel is a hexamer. (A) SDS-PAGE of N2a cells transiently transfected with GFP or CALHM1 with increasing concentrations of βME. (B) BN-PAGE of SH-SY5Y cells transiently transfected with CALHM1 under reducing and non-reducing conditions. Absence of lower molecular mass bands in reducing conditions (+βME) is likely due to altered structure of CALHM1 that allows the reduced protein to migrate through the gel quickly. Since the experiment was optimized to detect higher

order oligomers, monomeric CALHM1 likely runs through the gel. (C) Representative TIRF image of CALHM1-EGFP in oocyte plasma membrane acquired before photobleaching, showing fluorescent spots and regions of interest used to measure fluorescence intensity. (D) Representative fluorescence intensity traces from two fluorescent spots. Steps found using StepFinder (red line) are overlaid on the fluorescence intensity measurement (black line). After determining the number of steps in each bleaching trace, traces shown here were smoothed using 5-point running average for display purposes. (E) Distribution of the number of bleaching steps observed from CALHM1-EGFP expressing oocytes. Black data points are the average percentage of particles that bleached in each number of bleaching steps. Error bars indicate ± s.e.m. Data obtained from 271 particles, 8 imaging records and 3 oocytes were fitted with a binomial equation assuming the number of monomers in the complex, and with the percentage of fluorescent GFP molecules being a free parameter (colored, dashed lines). (F) Distribution of the number of bleaching steps observed using different methods to identify bleaching steps. The same traces that were analyzed using StepFinder and summarized in Fig. 3E (black bars) were also analyzed by visual inspection (red bars) to identify bleaching steps. Error bars indicate ± s.e.m.

FIGURE 4. Membrane topology of CALHM1. (A) Predicted membrane-spanning regions from 9 membrane topology prediction programs. (B) Model membrane topology of 4 TM domains, 3 cytoplasmic domains including the amino- and carboxyl-termini, and 2 extracellular domains. (C) CALHM1 is N-glycosylated at Asn140. Western blot of wild type CALHM1 reveals two bands, whereas CALHM1 with Asn140 mutated to alanine (N140A) reveals only the lower band, indicating that CALHM1 is glycosylated at Asn140, indicating extracellular localization. (D) The carboxyl terminus is cytoplasmic. Top: Permeabilized PC12 cells expressing CALHM1 were exposed to CALHM1 carboxyl-terminal antibody, revealing a positive immunostaining signal (right-center panel). Bottom: Unpermeabilized PC12 cells expressing CALHM1 exposed to same antibody had no immunostaining signal (right-center panel). Transfected cells were identified by EGFP expressed by the same vector. A similar strategy to localize the amino terminus was unsuccessful because insertion of an epitope tag prevented CALHM1 expression.

FIGURE 5. CALHM1 does not form gap junctions. (A) Representative images of dye transfer in N2a cells transiently-transfected with either GFP-tagged CALHM1 (top row) or GFP-tagged Cx30 (bottom row). In a group of transfected cells, a single cell was loaded with Alexa350 by a patch clamp whole-cell dialysis for 5 min (arrowhead). Fluorescence images were taken 5-60 min after loading to determine extent of Alexa350 transfer to other cells. (B) Percentage of injected cells that transferred dye to neighboring transfected cells. Only one of 12 dye-loaded CALHM1-transfected cells examined transferred dye, and to only one other cell, likely a daughter cell that has not yet completed cytokinesis (89), similar to that observed in the GFP-transfected cells. Conversely, 9 of 11 of the Cx30-transfected cells transferred dye to neighboring transfected cells. Furthermore, the dye was transferred to multiple cells in 6 of 8 cases. 8 GFP-expressing or untransfected, 11 Cx30-expressing, and 12 CALHM1-expressing cells were injected with dye. Statistical significance was determined using Fisher's Exact Test, $p < 0.001$. (C) Average number of cells into which dye transferred. The one injected control cell and one injected CALHM1-transfected cell that transferred dye transferred it to only one neighboring cell. Alternatively, when Cx30-transfected cells transferred dye, there were on average 2.44 recipient cells. Student's unpaired t-test with unequal variance, $p < 0.01$.

FIGURE 6. Schematic depiction of the alignment of the secondary structures of CALHM1, Panx1, Cx43, and Inx1. Conserved cysteines and glycosylation sites are also shown.

Table 1. Ionic Radii

Ion	Pauling Radius	Stokes Radius
Li^+	0.60	2.38
Na^+	0.95	1.84
K^+	1.33	1.25
Rb^+	1.48	1.18
Cs^+	1.69	1.19
TMA^+	3.47	2.05
TEA^+	4.00	2.82
TBA^+	4.94	4.72

Table 1. The ionic radii of monovalent cations. The Pauling and the Stokes radii (90) of each ion used to estimate the pore diameter of CALHM1 are shown.

Table 2. Molecular Dimensions of Fluorescent Dyes

	Lucifer Yellow	Alexa350	Alexa488	Alexa594	Alexa633
X	12.2	13.0	11.3	16.6	?
Y	**9.9**	**5.2**	**10.5**	**13.8**	**?**
Z	2.6	3.2	9	9.3	?
MW	443	350	570	760	~1150
Charge	-2	-1	-2	-2	?

Table 2. The molecular dimensions of fluorescent dyes. The unhydrated dimensions of each dye are shown. Since the molecules are not spherical, the median axial diameter was used to approximate the minimum diameter of the pore (30). This assumes that the longest axis aligns with the pore.

Figure 1

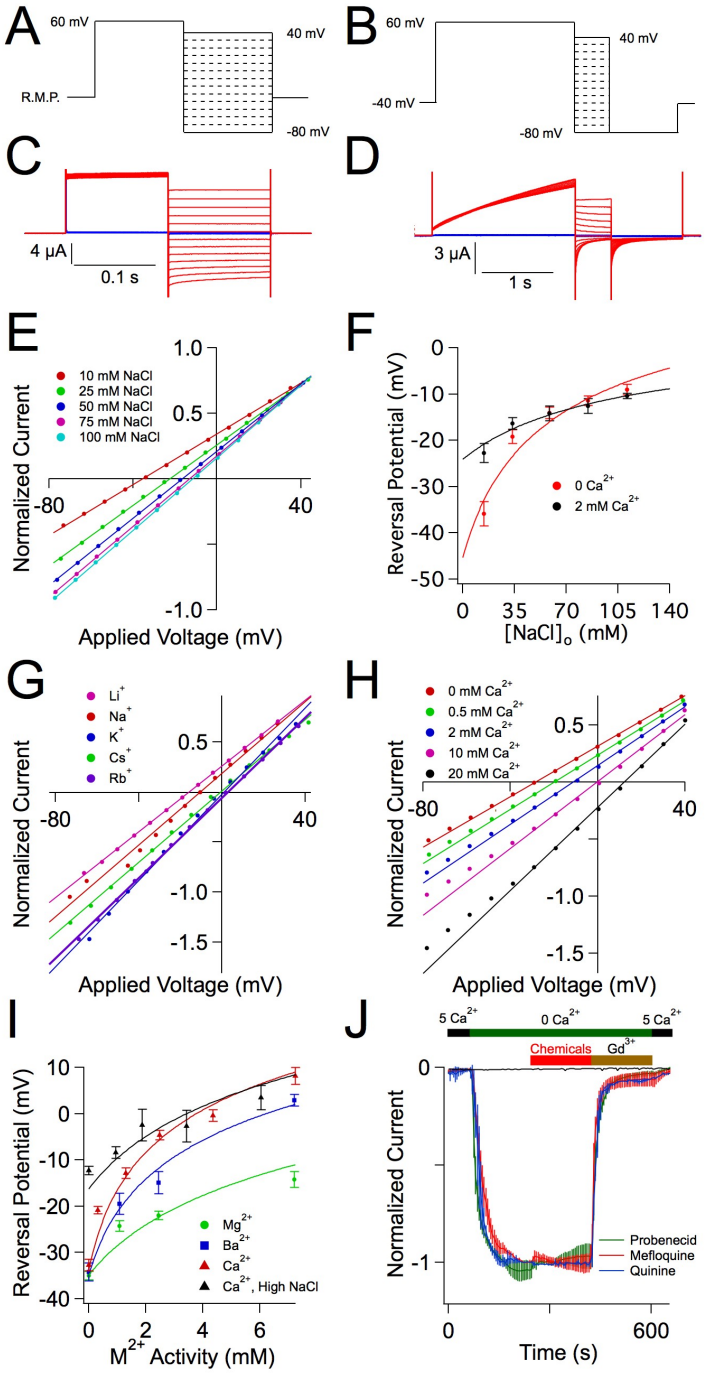

Figure 2

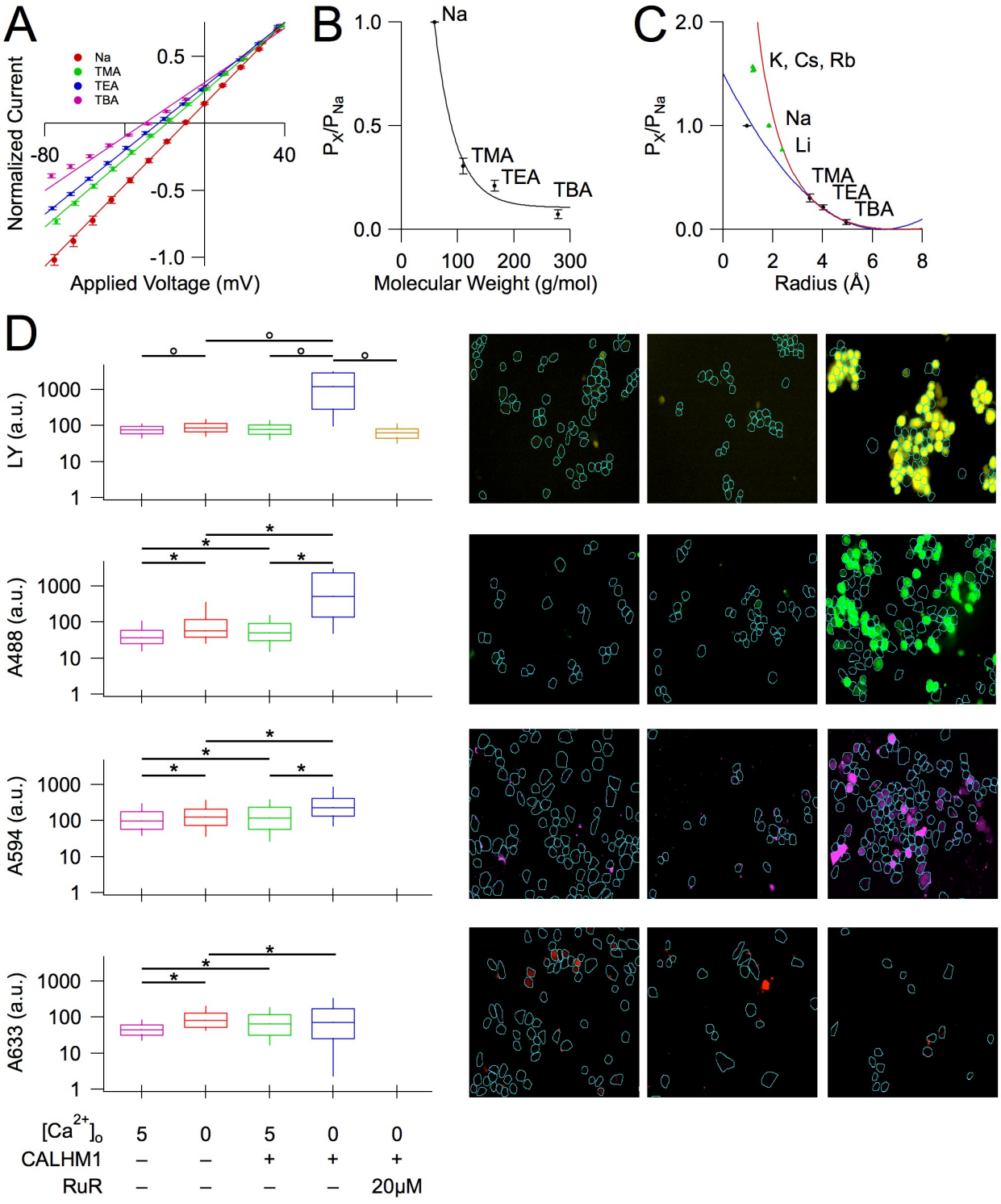

Figure 3

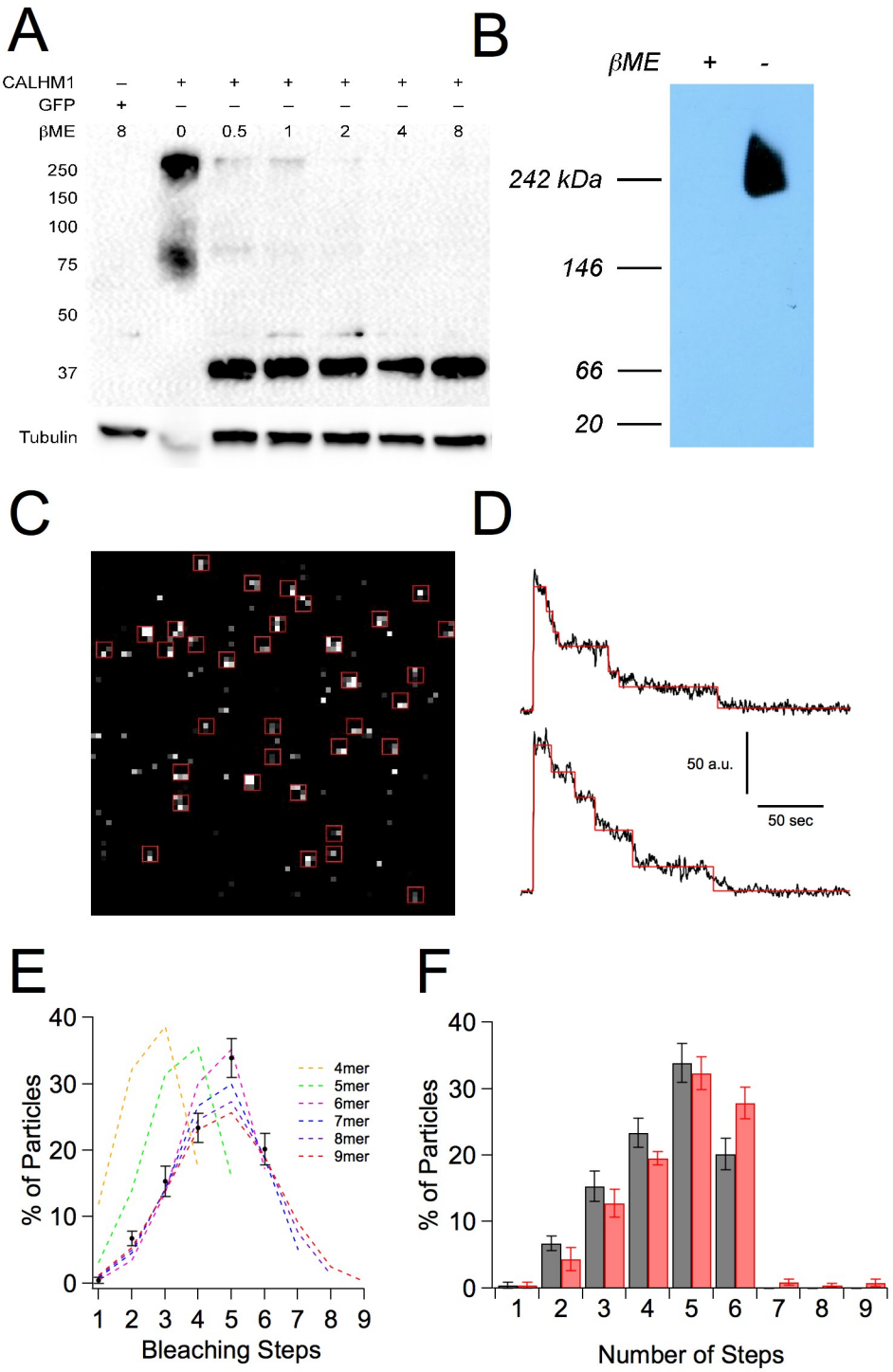

Figure 4

A

Program	# TM Domains	TM1	TM2	TM3		TM4	
TMHMM	3	19 - 38	48 - 70			186 - 205	
Toppred (KD)	4	18 - 38	52 - 72	103 - 123		186 - 206	
PHDhtm	4	21 - 38	51 - 70	102 - 122		184 - 201	
Tmpred	4	19 - 38	50 - 70	107 - 139		183 - 202	
SOSUI	4	15 - 37	50 - 72	112 - 134		192 - 214	
PSIpred	4	18 - 37	51 - 72	99 - 120		181 - 205	
HMMTOP	5	19 - 38	51 - 70	99 - 118	131 - 150	183 - 202	
SPLIT 4.0	5	20 - 35	51 - 73	98 - 120	124 - 139	182 - 203	
Toppred (GES)	6	18 - 38	52 - 72	99 - 119	123 - 143	182 - 202	260 - 280

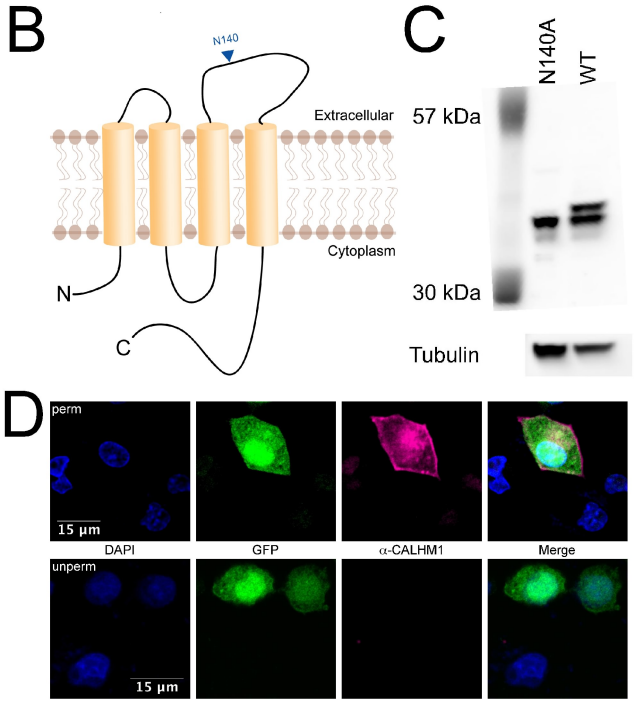

Figure 5

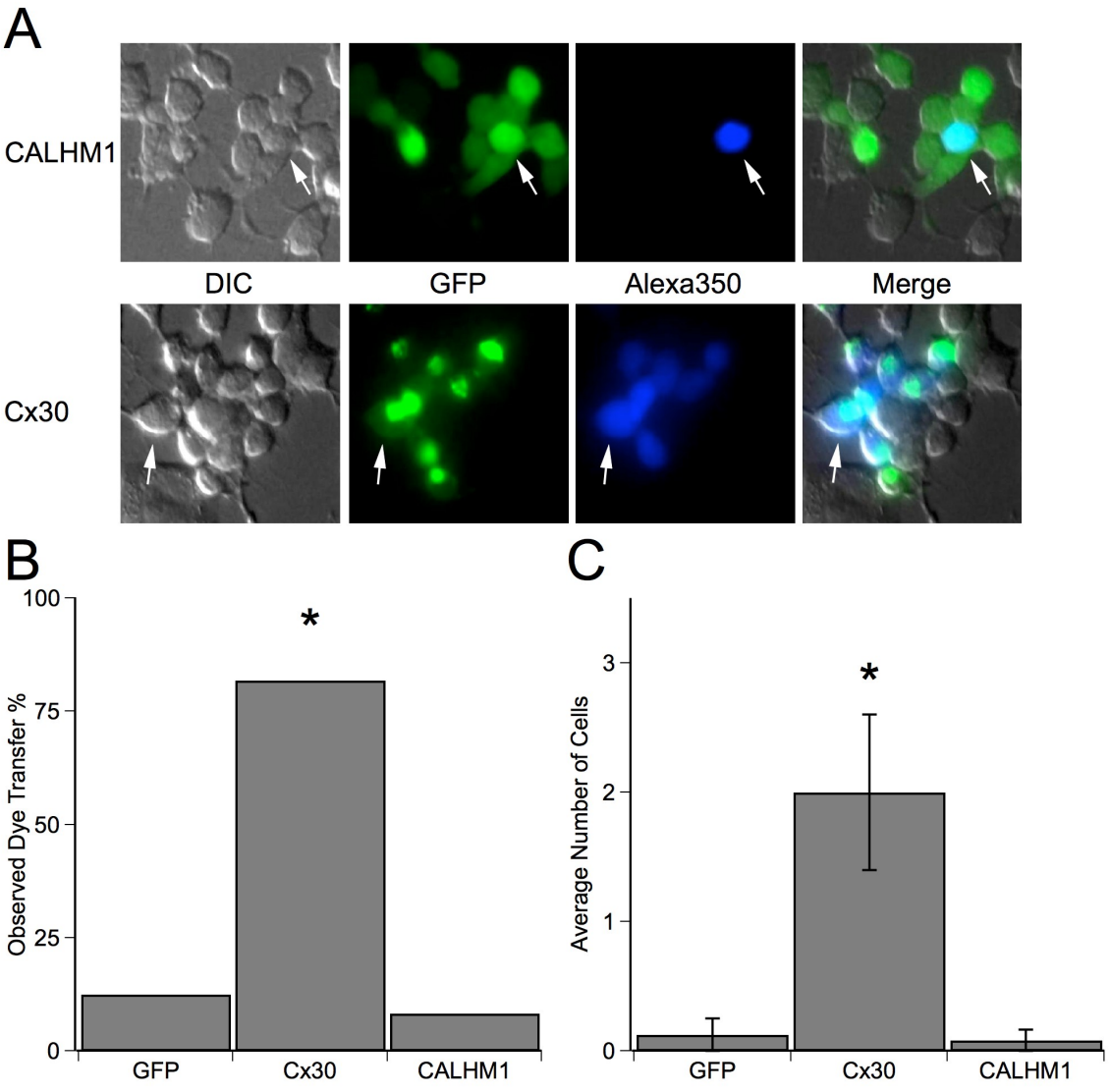

Figure 6